Unclassified
SECURITY CLASSIFICATION OF THIS PAGE

REPORT DOCUMENTATION PAGE

AD-A204 693

1b. RESTRICTIVE MARKINGS

3. DISTRIBUTION / AVAILABILITY OF REPORT
Approved for public release;
Distribution unlimited

2b. DECLASSIFICATION / DOWNGRADING SCHEDULE

4. PERFORMING ORGANIZATION REPORT NUMBER(S)
AFGL-TR-89-0040

5. MONITORING ORGANIZATION REPORT NUMBER(S)

6a. NAME OF PERFORMING ORGANIZATION
Air Force Geophysics Laboratory

6b. OFFICE SYMBOL (If applicable)
PHG

7a NAME OF MONITORING ORGANIZATION

6c. ADDRESS (City, State, and ZIP Code)
Hanscom AFB
Massachusetts 01731

7b ADDRESS (City, State, and ZIP Code)

8a. NAME OF FUNDING / SPONSORING ORGANIZATION

8b OFFICE SYMBOL (If applicable)

9 PROCUREMENT INSTRUMENT IDENTIFICATION NUMBER

8c. ADDRESS (City, State, and ZIP Code)

10 SOURCE OF FUNDING NUMBERS

PROGRAM ELEMENT NO.	PROJECT NO	TASK NO.	WORK UNIT ACCESSION NO.
61102F	2311	G5	02

11 TITLE (Include Security Classification)
Snapshots of High-Latitude Electrodynamics Using Viking and DMSP F7 Observations

12 PERSONAL AUTHOR(S) G.T. Marklund*; L.G. Blomberg*; K.Stasiewicz**; J.S. Murphree+; R. Pottelette#; L.J. Zanetti§; T.A. Potemra§; D.A. Hardy; F.J. Rich

13a. TYPE OF REPORT	13b. TIME COVERED	14. DATE OF REPORT (Year, Month, Day)	15 PAGE COUNT
REPRINT	FROM ____ TO ____	1989 February 17	14

16 SUPPLEMENTARY NOTATION * Dept of Plasma Physics, Royal Inst of Technology, Stockholm, Sweden ** Swedish Inst of Space Physics, Kiruna, Sweden; +Dept of Physics, University of Calgary, Alberta, Canada; # Centre de Recherces en Physique de l'Environment Terrestre et Planetaire, Saint-Maur-des-Fosses, France; § Applied Physics Lab, Johns Hopkins University, Laurel, MD

17. COSATI CODES		
FIELD	GROUP	SUB-GROUP

18 SUBJECT TERMS (Continue on reverse if necessary and identify by block number)
Aurora, Ionosphere, reprint, ~~DMSP~~, Viking

19 ABSTRACT (Continue on reverse if necessary and identify by block number)

Simultaneous observations by the Viking and the DMSP F7 satellites have been used as input to a new method to obtain snapshot pictures of the auroral electrodynamics. In particular, an "instantaneous" global equipotential (or convection) pattern is calculated from distributions of field-aligned current and conductivity which are qualitatively consistent with the Viking auroral imager data and quantitatively consistent with magnetic field and particle data from the two satellites. This convection pattern, which is of the normal two-cell type, with a weak dusk cell and a strong, elongated crescent-shaped dawn cell (consistent with positive interplanetary magnetic field B_y), agrees well with the Viking electric field data. The model and the observed potential profiles agree nicely along the entire Viking orbit except for two intervals above acceleration regions where deviations are to be expected (due to parallel electric fields). These regions are characterized by U-shaped potential minima, upward field-aligned currents, upgoing ion beams, and relatively intense auroral kilometric radiation. Thus, the model results are consistent with the Viking observations not only on a global scale but also on the scale of the auroral acceleration regions. The corresponding convection in the magnetosphere is obtained from a simple projection to the equatorial plane of the deduced two-cell convection pattern. From this the location of the plasmapause is inferred.

20 DISTRIBUTION / AVAILABILITY OF ABSTRACT
☐ UNCLASSIFIED/UNLIMITED ☒ SAME AS RPT. ☐ DTIC USERS

21 ABSTRACT SECURITY CLASSIFICATION
Unclassified

22a. NAME OF RESPONSIBLE INDIVIDUAL
Frederick Rich

22b. TELEPHONE (Include Area Code)

22c. OFFICE SYMBOL
AFGL/PHG

DD FORM 1473, 84 MAR 83 APR edition may be used until exhausted.
All other editions are obsolete.

SECURITY CLASSIFICATION OF THIS PAGE
Unclassified

CONT OF BLOCK 16:

Reprinted from J of Geophysical Research, Vol 93, #A12, pp 14,479-14,492, 1 Dec 1988

JOURNAL OF GEOPHYSICAL RESEARCH, VOL. 93, NO. A12, PAGES 14,479–14,492, DECEMBER 1, 1988

Snapshots of High-Latitude Electrodynamics Using Viking and DMSP F7 Observations

G. T. MARKLUND,[1] L. G. BLOMBERG,[1] K. STASIEWICZ,[2,3] J. S. MURPHREE,[4] R. POTTELETTE,[5] L. J. ZANETTI,[6] T. A. POTEMRA,[6] D. A. HARDY,[7] AND F. J. RICH[7]

Simultaneous observations by the Viking and the DMSP F7 satellites have been used as input to a new method to obtain snapshot pictures of the auroral electrodynamics. In particular, an "instantaneous" global equipotential (or convection) pattern is calculated from distributions of field-aligned current and conductivity which are qualitatively consistent with the Viking auroral imager data and quantitatively consistent with magnetic field and particle data from the two satellites. This convection pattern, which is of the normal two-cell type, with a weak dusk cell and a strong, elongated crescent-shaped dawn cell (consistent with positive interplanetary magnetic field B_y), agrees well with the Viking electric field data. The model and the observed potential profiles agree nicely along the entire Viking orbit except for two intervals above acceleration regions where deviations are to be expected (due to parallel electric fields). These regions are characterized by U-shaped potential minima, upward field-aligned currents, upgoing ion beams, and relatively intense auroral kilometric radiation. Thus, the model results are consistent with the Viking observations not only on a global scale but also on the scale of the auroral acceleration regions. The corresponding convection in the magnetosphere is obtained from a simple projection to the equatorial plane of the deduced two-cell convection pattern. From this the location of the plasmapause is inferred.

1. INTRODUCTION

In our efforts to better understand the magnetosphere-ionosphere system a major problem is to provide an acceptable coverage by simultaneous observations within the large volume to be studied. The high-latitude ionosphere acts in many respects as a projection screen for processes taking place in the outer magnetosphere and boundary regions. Much can therefore be learnt from studies of the electrodynamics of the high-latitude ionosphere, which is a relatively small and rather accessible region. Joint efforts to combine simultaneous observations by different spacecraft and/or ground-based facilities have become relatively common recently. The problem at hand is how to utilize the information from the various observations to reconstruct, on a global scale, the instantaneous distributions of all relevant electrodynamical parameters in a self-consistent manner.

Numerous simulation studies of the interaction between the global ionospheric electric field, currents, and conductivities have been presented. In such models, two of the quantities are specified, and the third is calculated from these. The chosen input quantities are typically the ionospheric conductivity combined with either the ionospheric potential or the ionospheric or field-aligned current [e.g., *Nisbet et al.*, 1978; *Kamide and Matsushita*, 1979a,b; *Bleuler et al.*, 1982; *Marklund et al.*, 1985]. The conductivity model is crucial in models of this kind [cf. *Reiff*, 1984] and can therefore not be chosen without taking into account the physical coupling between the conductivity and the other specified input, e.g., the field-aligned current. This has usually been overlooked in studies of this kind with a few exceptions [e.g., *Mishin et al.*, 1986]

From observations it is clear that an enhancement in the upward field-aligned current is usually accompanied by an enhancement in the ionization or the conductivity. Although the enhancements of these quantities are typically caused by particles belonging to different energy ranges, such a relationship exists, and it is important to take it into account in the modeling. The importance of the coupling between the conductivity and the upward field-aligned current is treated in detail in a special report [*Blomberg and Marklund*, 1988a].

During the last decade, efforts have been made to coordinate observations obtained simultaneously by spacecraft and ground-based instrumentation in order to obtain global snapshots of some parameter, often the electric field or the ion drift. Schematic convection patterns have in this way been constructed for the nightside high-latitude ionosphere [*Heelis et al.*, 1983] and for the dayside ionosphere [*Marklund et al.*, 1986].

A combination of this latter approach (based on coordination of simultaneous observations) with that using global numerical simulations results in a potentially extremely useful way to better understand the instantaneous behavior of the magnetosphere-ionosphere system. This is so, because not only one single parameter (e.g., the ion convection as exemplified above) but all electrodynamical parameters are in a self-consistent way included in such an approach. In this context the auroral UV-imaging instruments found on polar-orbiting satellites such as Dynamics Explorer 1, Hilat,

[1] Department of Plasma Physics, Royal Institute of Technology, Stockholm, Sweden.
[2] Swedish Institute of Space Physics, Kiruna, Sweden.
[3] Now at Swedish Institute of Space Physics, Uppsala, Sweden.
[4] Department of Physics, University of Calgary, Calgary, Alberta, Canada.
[5] Centre de Recherches en Physique de l'Environnement Terrestre et Planétaire, Saint-Maur-des-Fossés, France.
[6] Applied Physics Laboratory, Johns Hopkins University, Laurel, Maryland.
[7] Space Physics Division, Air Force Geophysics Laboratory, Bedford, Massachusetts

Paper number 88JA03093.
0148-0227/88/88JA-03093$05.00

and Viking play a crucial role. The global view of the aurora provides a natural reference frame for the other observations and the modeling, and it reveals important information on the electrodynamical state of the different parts of the auroral ionosphere.

Kamide et al. [1986] used images of auroral emissions observed by Dynamics Explorer 1 to calculate high-latitude ionospheric conductivities. By combining these with simultaneous ground-based magnetometer data they were able to estimate on a global scale the distributions of ionospheric electric fields and currents, field-aligned currents, and Joule heating with a time resolution of 12 min.

In the present paper, a new and different method to obtain snapshots of the auroral electrodynamics on a global scale will be described, using auroral UV images and in situ observations of fields and particles (and/or remote observations of the same or related parameters by ground-based instrumentation). A preliminary and brief description of this new technique was given in the paper by *Marklund et al.* [1987].

In the present paper the new technique and numerical model are described in much more detail. Furthermore, a number of significant improvements and additions have been made in the analysis of the particular event chosen to illustrate the new method. The most important ones are as follows:

1. We included, in addition to the Viking data, magnetic field and particle data from a noon–midnight auroral oval crossing by the DMSP F7 satellite. As a result of this, all information used to calibrate the model input data was obtained within 15 min for the dayside oval and 27 min for the entire auroral oval.

2. We included additional data from the other experiments on Viking (particle and high-frequency wave experiments) which made possible a detailed investigation of two auroral acceleration regions (including electric field, current, particle, and wave signatures). Furthermore, a more detailed estimate of the downward electron energy flux at the ionospheric level could be made.

3. We calculated the $\mathbf{E} \times \mathbf{B}$ drifts from the Viking electric field data which allowed a two-dimensional comparison with the model convection pattern.

4. We calculated the ionospheric currents, Joule power dissipation, and convection in the equatorial plane of the magnetosphere.

Section 2 outlines the main principles of how to construct the model input data from the observations. Section 3 describes the numerical model (in particular the choice of conductivity model). The auroral situation, the geophysical conditions, and the geometry of the oval are described in section 4. Section 5 presents the observations, model input distributions, and results of the model calculations. Discussion and summary of the results are presented in sections 6 and 7, respectively.

2. METHODOLOGY

The basic elements needed to infer and calibrate the model input data and check the output data, following the procedure used here, are (1) one or several UV images showing clearly the auroral emissions along the entire auroral oval as well as in the polar cap, (2) in situ observations of electric and magnetic fields and auroral particles from polar-orbiting satellites (at least one), preferably supplemented by remote observations of these or related parameters by ground-based facilities such as incoherent or coherent scatter radars and magnetometer networks, (3) experience of the statistical patterns of field-aligned currents and ionospheric conductivities and the observed coupling between these for different geophysical conditions, as reported in the literature, and (4) a sophisticated numerical model to solve the elliptical equation that relates the ionospheric potential (model output) to the ionospheric conductivity and field-aligned current distributions (model input).

The task is to reconstruct on a global scale the distributions of all relevant electrodynamic parameters associated with the particular auroral situation given by the UV image. To accomplish this, global input distributions of conductivities and magnetic field-aligned currents have to be inferred from and made consistent with the direct observations and fed into the numerical model to obtain the potential, which is finally checked against the observations.

The Auroral UV Image

The auroral distribution viewed by the UV imager is used to obtain a global reference frame for the other observations and in particular to locate the regions of active intense auroras. These are clearly associated with enhanced upward field-aligned currents and ionospheric conductivities. The coupling between these quantities is represented here by the linear relationship expressed by equation (10) below (in section 3).

The UV images also reveal much fine structure both in the intense auroral structures and in the weaker and diffuse "background" auroral oval. The fine structure in the auroral emissions has not been taken into account in the global modeling for several obvious reasons. (1) There are several difficulties involved in trying to obtain reliable absolute intensities from the UV image. For example, corrections have to be made for effects of the oblique viewing angle of the imager and for different contrasts in different parts of the auroral oval. (2) The errors arising from trying to take the fine structure of the diffuse background auroral oval into account in the modeling would most likely be comparable to (or even larger than) the real intensity variations. (3) Even if it would be possible, in principle, to infer some fine structure in the ionospheric conductivity from the UV image, this would not improve the modeling unless the field-aligned current distribution could be inferred with a corresponding spatial resolution (which is clearly not possible).

We have therefore chosen to represent the diffuse "background" auroral oval by statistical patterns of conductivities and field-aligned currents . The MLT dependence of this field-aligned current distribution is taken from *Iijima and Potemra* [1976a, 1978], while its location is chosen in consistency with the UV image.

To summarise, the UV image is used to obtain information on the size, shape, and width of the oval as a general frame of reference for the other observations and for the modeling. Moreover, the UV image is used to identify the location and extent in latitude and local time of the more intense auroral emissions along the oval. Statistical patterns of field-aligned current represent the current system associated with the diffuse aurora, and the corresponding conductivity distribution is given by the Gaussian-shaped, "oval centered," term modified by enhancements in the regions of statistical upward field-aligned currents. In addi-

tion to this, the current and conductivity in regions where active aurora is found from the image are enhanced. Note that for both these contributions, the current and conductivity are treated in a consistent manner in the sense that part of the conductivity distribution is coupled to the field-aligned current (cf. section 3). Moreover, the field-aligned current and the conductivity distribution are chosen so as to be everywhere continuous. The center latitude between the region 1 and region 2 field-aligned currents and that of the peak background conductivity coincide in the model with the center latitude of the auroral oval as observed by the UV imager.

Calibration of the Model Input

The rough and qualitative picture of the model input distributions resulting from the procedure above will now be refined and calibrated to fit with the actual measurements (in situ and/or remote). For the sake of convenience, the calibration procedure will be described here using satellite observations, although it applies equally well to ground-based observations. Magnetic field and particle data are used to calculate the distributions of field-aligned currents and particle energy flux along the satellite orbit. These estimates have to be multiplied with the appropriate scaling factors between the satellite altitude and the ionosphere. In this study we have used the scaling factors obtained from a pure dipole magnetic field.

The particle energy flux is used to calculate the contribution from precipitating particles to the ionospheric conductivity as expressed by the formula $\Sigma_P' = a\Gamma^{1/2}$ from *Harel et al.* [1981] where a is a proportionality constant and Γ the particle energy flux. Another, perhaps more accurate way to calculate Σ_P' is to use the dissipation algorithm for electrons, given by *Rees* [1963] assuming a balance between ionization and recombination losses. Since Σ_P' does not represent the total conductivity but only the contribution due to the precipitating particles, it should be used to calibrate the corresponding part of the model conductivity (i.e., excluding the contribution to the conductivity from solar EUV radiation; see section 3).

For orbits or segments of orbits for which there is a good large-scale correlation between orthogonal components of the electric field (**E**) and the residual magnetic field, **b**, the total ionospheric conductivity, Σ_P, can be inferred [*Sugiura*, 1984] according to the following expression: $\Sigma_P = \Delta b/\mu_0 \Delta E$. This constitutes another possible way to calibrate the model input conductivity.

Calibration of the model input data is now possible using these estimates of the field-aligned current and height-integrated conductivity distributions. Note that all model coefficients related to the background conductivity (cf. section 3) are position-independent. Thus, the calibration of the background conductivity is, with necessity, made globally.

For regions covered by the satellite orbit the model currents and conductivities are matched to the observed widths of the large-scale current sheets and particle precipitation regions and to the typical magnitudes of these parameters. No attempt has been made to represent the observed fine structure in the model input data.

For active regions not covered by the satellite orbit(s), both the region 1 and region 2 large-scale model currents are enhanced so that their amplitudes are consistent with either (1) current magnitudes measured in some nearby active auroral structure with a similar UV emission intensity or (2) typical current magnitudes, based on the experience from earlier satellite measurements over similar auroral structures.

The region 2 to region 1 current ratio will in this way assume a lower value in the regions of low activity (namely the ratio specified by the quiet time statistical patterns of *Iijima and Potemra* [1976a, 1978]) than in the regions of active aurora where this ratio approaches unity.

Since the field-aligned current and the conductivity are coupled in the model, as represented by one of the terms in the expression for the conductivity (cf. section 3), the calibration of the conductivity becomes an iterative process during which a better estimate of the proportionality factor in equation (10) will evolve. A complete description of the conductivity model is given in section 3.

Model Output and Check Procedure

Once the model input data are specified, they are fed into the numerical model (described in section 3) which calculates the global ionospheric potential distribution. Before presenting the potential pattern as it comes out from the calculation the result is to be checked against measurements in the same way as the model input data.

Electric field (or ion drift) observations are used to calculate both the potential variation and the $\mathbf{E} \times \mathbf{B}$ drift pattern along the projected satellite orbits (or radar tracks), which allows point-by-point comparisons with the model result.

Since the strengths of the field-aligned currents (and the corresponding conductivity) in active auroral regions not covered by the satellite are assumed rather than measured, they could be varied in such a way that a better fit is obtained between the measured and computed potential variation. Note, however, that such a variation in the current strength of, say, a nightside auroral structure will have only minor influence on the dayside potential pattern provided that not too extreme current values have been used. More locally, the effects are, however, significant and could be used for improvement of the model input data.

The resulting global pattern can be used to predict the electric field or convection velocity along the ionospheric foot point of any satellite trajectory or radar track which enables direct point-by-point comparisons with observations. This should be extremely useful in, for example, coordinated multiradar-multisatellite studies of the global convection. In such a case, with a relatively dense network of observations, the iterative procedure, to improve successively the fits between the measured and computed potential variations along the different satellite trajectories (or radar tracks), as described above, should be most valuable.

Combining the electric field given by the final potential pattern with the model conductivity allows both the ionospheric currents and the Joule power dissipation to be calculated according to equations (1) and (11) below. The effect of these calculated ionospheric currents at the ground level can be estimated, to be used for direct comparisons with data from ground-based magnetometers. This represents another possible way to check the model data.

An important feature of the new technique presented here is that all relevant electrodynamical parameters involved in the modeling, namely the electric field, the field-aligned currents, and the conductivities, are treated self-consistently

and checked or calibrated point by point against direct measurements in an interactive way not done before.

3. MODEL EQUATIONS

The calculation of the potential distribution has been performed using spherical (surface) coordinates, where the θ coordinate corresponds to magnetic colatitude and the ϕ coordinate is related to magnetic local time (MLT).

The basic equation relating the height-integrated ionospheric (horizontal) current ($\mathbf{J}_0$) to the ionospheric electric field ($\mathbf{E}_0$) can be written

$$\mathbf{J}_0 = \boldsymbol{\Sigma} \cdot (\mathbf{E}_0 + \mathbf{v}_n \times \mathbf{B}) \tag{1}$$

where $\mathbf{E}_0$ is the electric field in the Earth-fixed frame and $\mathbf{v}_n$ is the velocity of the neutral wind, which in the calculation below has been assumed to be zero. Note that the electromotive force $\mathbf{v}_n \times \mathbf{B}$ does not significantly influence the field-aligned current [cf. *Lyons and Walterscheid*, 1986].

$\boldsymbol{\Sigma}$ is the height-integrated horizontal conductivity tensor

$$\boldsymbol{\Sigma} = \begin{bmatrix} \Sigma_{\theta\theta} & \Sigma_{\theta\phi} \\ \Sigma_{\phi\theta} & \Sigma_{\phi\phi} \end{bmatrix} \tag{2}$$

Its components (except at equatorial latitudes) are given by

$$\Sigma_{\theta\theta} = \Sigma_P / \sin^2 I \tag{3a}$$

$$\Sigma_{\theta\phi} = -\Sigma_{\phi\theta} = \Sigma_H / \sin I \tag{3b}$$

$$\Sigma_{\phi\phi} = \Sigma_P \tag{3c}$$

where I is the inclination of the geomagnetic field ($\mathbf{B}$) (approximated by a dipole) and Σ_P and Σ_H are the height-integrated Pedersen and Hall conductivities, respectively.

The height-integrated horizontal current and the field-aligned current (positive downward) are related through

$$\nabla \cdot \mathbf{J}_0 = j_\parallel \cdot \sin I \tag{4}$$

$$\nabla \cdot (\boldsymbol{\Sigma} \nabla \Phi) = -j_\parallel \cdot \sin I \tag{5}$$

This equation forms the basis for solving (numerically) the electrostatic potential once the field-aligned current and the conductivity are specified.

The boundary condition used in the calculation is $\Phi(\theta = 90^\circ, \phi) = 0$; i.e., the magnetic equator is an equipotential surface.

In the present model the ordinary region 1 and region 2 field-aligned currents [cf. *Iijima and Potemra*, 1976a, 1978], as well as the cusp currents [*Iijima and Potemra*, 1976b] can be represented. The basic parameters defining the geometry of the current systems are θ_{00}, colatitude of the dayside region 1 / region 2 interface; $\Delta\theta_0$, difference between nightside and dayside interface latitudes; and $\Delta\theta_1$, $\Delta\theta_2$, $\Delta\theta_C$, the latitudinal widths (in degrees) of region 1, region 2, and cusp currents, respectively.

The center of the auroral oval (assumed to coincide with the region 1 / region 2 interface) is described in this study by

$$\theta_0 = \theta_{00} + \Delta\theta_0 \cdot \left| \cos \frac{15^\circ \cdot \mathrm{MLT}}{2} \right| \tag{6}$$

The height-integrated conductivities are represented by

$$\Sigma_P = \sqrt{\Sigma_{0P}^2 + \Sigma_{gP}^2 + \Sigma_{UVP}^2 + \Sigma_{j_\parallel P}^2} \tag{7a}$$

$$\Sigma_H = \sqrt{\Sigma_{0H}^2 + \Sigma_{gH}^2 + \Sigma_{UVH}^2 + \Sigma_{j_\parallel H}^2} \tag{7b}$$

The root-sum-square relation is employed, since the various ionisation processes giving rise to the conductivity take place roughly within the same altitude range, and hence, as discussed by, for example, *Wallis and Budzinski* [1981], addition of the ionisation rates (which if balanced by recombination are proportional to n_e^2) gives a far more accurate estimate of the total conductivity (proportional to n_e) than a direct summation of the different conductivity contributions.

Σ_0 is a background term having a constant low value, representing the contribution from cosmic radiation and galactic EUV. The exact magnitude of this term is not critical to the modeling and has in this study been given the value 0.5 S.

Σ_g represents an average auroral zone background conductivity given by

$$\Sigma_g = \Sigma_{g0} \exp\left(-\frac{(\theta - \theta_0)^2}{\theta_{g0}^2} \right) \tag{8}$$

centered around the colatitude θ_0 (coinciding with the center of the auroral oval) and having a characteristic half width of θ_{g0} degrees.

Σ_{UV} represents the part of the conductivities which is produced by solar EUV radiation. It is given here by

$$\Sigma_{UV} = \alpha \sqrt{\cos \chi} \tag{9}$$

where χ is the solar zenith angle and α a proportionality factor. The value of α is taken from *Vickrey et al.* [1981].

$\Sigma_{j_\parallel}$ represents the conductivity enhancement produced by precipitating electrons associated with upward field-aligned currents. In the present model a relationship between the field-aligned current and the conductivity has been used, such that the conductivity peaks in regions of upward current. The form of this relation is

$$\Sigma_{j_\parallel} = \begin{cases} k(\mathrm{MLT})|j_\parallel| & j_\parallel \text{ upward} \\ 0 & j_\parallel \text{ downward} \end{cases} \tag{10}$$

The factor of proportionality k(MLT) is here chosen to be dependent of local time in order to account for the differences in the hardness of the particle spectrum. Thus, it has a lower value on the dayside, where the precipitation generally is softer than on the nightside. In the morning and evening sectors there is a smooth transition between the two extreme values. The transition region stretches over 2 hours of magnetic local time. The contribution from protons to the total precipitated particle energy is estimated to be at most 10 to 20 per cent [*Hultqvist*, 1973] and is assumed here to be accounted for by Σ_g. An important parameter in the modeling is the Hall to Pedersen conductivity ratio Σ_H/Σ_P, which, in principle, should be slightly different for the various terms in the conductivity model (cf. equation (7)) due to different ionisation mechanisms. The ratio between the total Σ_H and Σ_P used in this study is 1.7 within the auroral oval and close to 1.0 in the nightside polar cap

TABLE 1. Model Input Parameter Values

Geometry of the $j_\parallel$ Model Currents	
θ_{00}	$= 14°$
$\Delta\theta_0$	$= 12°$
ΔR_1	$= \Delta R_2 = 3°$
ΔR_C	$= 2°$
Conductivity Model	
Σ_{0P}	$= 0.5$ S
$\Sigma_{\varepsilon 0P}$	$= 5$ S
θ_0	$= 14°$ at 1200 MLT
$\theta_{\varepsilon 0}$	$= 3°$ (cf. equation (8))
α_P	$= 5$ S (cf. equation (9))
k_P	$= \begin{cases} 2\ \mathrm{S}/(\mu\mathrm{A/m^2}), & \text{on dayside} \\ 13\ \mathrm{S}/(\mu\mathrm{A/m^2}), & \text{on nightside} \end{cases}$
Σ_H/Σ_P	$= \begin{cases} 1, & \text{for } \Sigma_0 \\ 1.7, & \text{for } \Sigma_\varepsilon,\ \Sigma_{UV}, \text{ and } \Sigma_{j_\parallel} \end{cases}$
Corotation Potential	
p	$= 8.1 \times 10^{22}$ Am^2 (cf. equation (12))
ω	$= 2\pi/(24 \times 3600)$
θ_{NP}	$= 11°$ (cf. equation (13))
UT	$= 0800$

For explanation, see section 3.

and subauroral regions using the parameter values listed in Table 1.

Once the ionospheric potential is calculated from equation (5), the associated electric field and the height-integrated conductivity can be used to calculate the ionospheric current, $\mathbf{J}_0$, given by (1) and the Joule power dissipation, P_{Joule}, given below:

$$P_{\mathrm{Joule}} = \mathbf{E} \cdot \boldsymbol{\Sigma} \cdot \mathbf{E} = \Sigma_{\theta\theta} E_\theta^2 + \Sigma_{\phi\phi} E_\phi^2 \qquad (11)$$

The ionospheric potential, Φ, can be projected onto the magnetospheric equatorial plane under the assumption of perfect mapping (no magnetic field-aligned electric fields). In the present study a simple centered dipole field has been used.

The electrostatic potential or the electric field can be given in either the corotating frame of reference (assumed to be identical to the frame where $\mathbf{v}_n = 0$) or in a coordinate system defined by the magnetic axis and the direction to the Sun (Sun-fixed frame). The geographic north pole can be regarded as rotating around the magnetic pole at a magnetic colatitude of 11° with a 24-hour period. The corotation potential (or corotation electric field) needed for transformation between the two frames will therefore be UT-dependent.

To account for this in the model an expression has been derived for the UT-dependent corotation electric field, which in turn has been used to obtain a "pseudo-potential," Φ_C, which approximates the effect of the UT-dependence of the corotation field. This "pseudo-potential" reads:

$$\Phi_C(\theta,\phi) = \frac{\mu_0 p}{4\pi}\frac{\omega}{r}\left[\sin\theta_{NP}\cos(\phi_{NP}-\phi)\left(\theta + \frac{\sin 2\theta}{2}\right) - \cos\theta_{NP}\sin^2\theta\right] \qquad (12)$$

where p is the magnetic dipole moment ($= 8.1 \times 10^{22}$ Am^2); ω is the angular velocity of the Earth's rotation; r is the geocentric distance; and θ and ϕ are magnetic colatitude and local time, respectively, with subscript NP referring to the geographic north pole. The latter are approximately given by

$$\theta_{NP} \approx 11° \qquad (13a)$$

$$\phi_{NP} \approx 15 \cdot \mathrm{UT} + 111° \qquad (13b)$$

An exhaustive treatment of the corotation field and its UT-dependence will be the subject of a future study. For a further description of the numerical method, see *Blomberg and Marklund* [1988*b*]. The values of the model parameters used for this study are summarized in Table 1 .

4. GEOPHYSICAL CONDITIONS

Figure 1 shows the northern hemisphere auroral oval as viewed by the UV imager experiment on Viking at 0724 UT during orbit 360, April 28, 1986. The auroral oval was crossed by Viking in roughly a dusk-dawn orbit and by DMSP F7 in roughly a noon-midnight orbit, as shown by the inserted ionospheric foot points of the two satellites.

Three localised bright auroral structures can be recognised in the evening and midnight sector, the largest one centered at about 65° invariant latitude, 0100 magnetic local time (MLT) with an east-west extent of roughly 20°. The western edge of the bright spot around 2130 MLT was crossed by the DMSP F7 satellite, as will be shown below. Relatively bright dayside auroras are seen in the prenoon sector, whereas the remaining part of the auroral oval has a relatively smooth and regular luminosity distribution. Note that the auroral oval in the early morning sector nearly coincides with the limb of the Earth. This implies that the weak emission intensities observed in this region may not be due entirely to auroral precipitation.

The afternoon sector of the auroral oval was traversed by Viking around 0724 UT, i.e., the time the UV image was taken. The prenoon sector of the auroral oval was traversed by the DMSP F7 satellite around 0739 UT; i.e., all information used to reconstruct the dayside model input data was obtained roughly within a 15-min interval.

Of the nightside auroral activity, the bright spot centered around 2130 MLT was traversed by the DMSP F7 satellite around 0750 UT, which allowed a calibration of the model input data for this part of the nightside oval within less than half an hour after the UV image was taken.

The *AE* index for this time period [*National Space Science Data Center*, 1986] shows that after a period of growth in the electrojet intensity previous to the UV image, it remained at a high but relatively stable value around 500 nT during the calibration time period 0724 - 0751 UT and then declined to about 400 nT as Viking traversed the prenoon auroral oval around 0900 UT.

We have chosen this particular event to illustrate in some detail how to use the new technique to reconstruct the electrodynamics associated with a given auroral situation viewed by a UV imager. The assumption made to enable such a reconstruction on a global scale is that the auroral and geophysical conditions remained relatively stable during the time period used for the calibration of the model input data, i.e., between 0724 UT and 0750 UT (for the dayside auroral oval between 0724 UT and 0739 UT). Since in situ observations of the nightside auroral activity are available only from one oval crossing (DMSP F7, 2130 MLT, 0739 UT) as com-

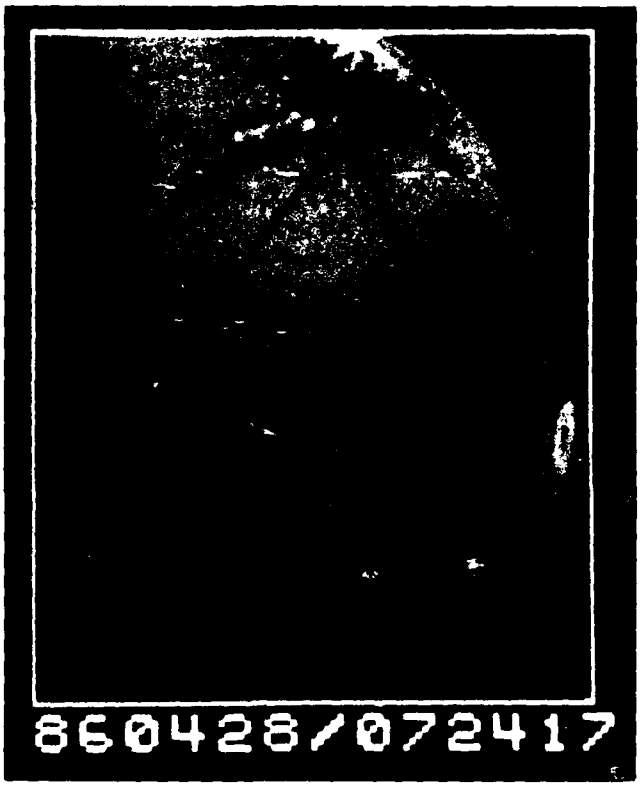

Fig. 1. The northern hemisphere auroral oval as viewed by the UV imager experiment on Viking at 0724 UT, orbit 360, April 28, 1986.

pared to three on the dayside, the possibility of calibrating the input data and checking the stability is smaller there. The DMSP F7 observations of strongly enhanced particle precipitation and field-aligned currents (which will be presented below) at the same location at which the intense and relatively narrow auroral structure around 2130 MLT was observed by the UV imager 27 min earlier speak in favor of a less violent nightside auroral activity during this time period.

No IMP 8 interplanetary magnetic field (IMF) data exist for this time period, but data from the Greenland magnetometer chain indicate that the IMF B_y component was positive during this event (E. Friis-Christensen, private communication, 1987).

5. Results and Comparisons With Viking and DMSP F7 Satellite Data

Figure 2 shows the input Σ_P and $j_\parallel$ distributions, which are qualitatively consistent with the auroral image seen in Figure 1 and, as will be shown below, in good quantitative agreement with the Viking and DMSP F7 data.

The region 1 and region 2 current patterns of *Iijima and Potemra* [1976a, 1978], representative for the diffuse quiet time auroral oval, are seen to be modified by (1) current enhancements in the local time sectors associated with the bright auroral structures identified from Figure 1 and (2) cusp current sheets, inferred from the Viking magnetic field observations (see below) with location and extent in accordance with the observations by *Iijima and Potemra* [1976b]. Since both the upward and downward currents associated with a bright auroral structure are assumed to be enhanced, the $j_\parallel$ contours will look relatively symmetric about the noon-midnight plane in contrast to the Σ_P distribution, which is seen to have a relatively higher magnitude in the regions of upward field-aligned currents (as a result of the current-conductivity coupling term) with intense maxima in the bright auroral forms. The ionisation contribution from solar EUV gives rise to the day-night conductivity gradient.

The two projected orbits are seen to cross the prenoon auroral oval (region 1 and region 2) relatively close and to cross each other almost at the center of the prenoon cusp current sheet. The 1-hour time separation between the two satellites at this location allows us to check the time stability of this prenoon triple current sheet (see below). Note that the DMSP F7 satellite passed through the intense bright auroral form around 2130 MLT.

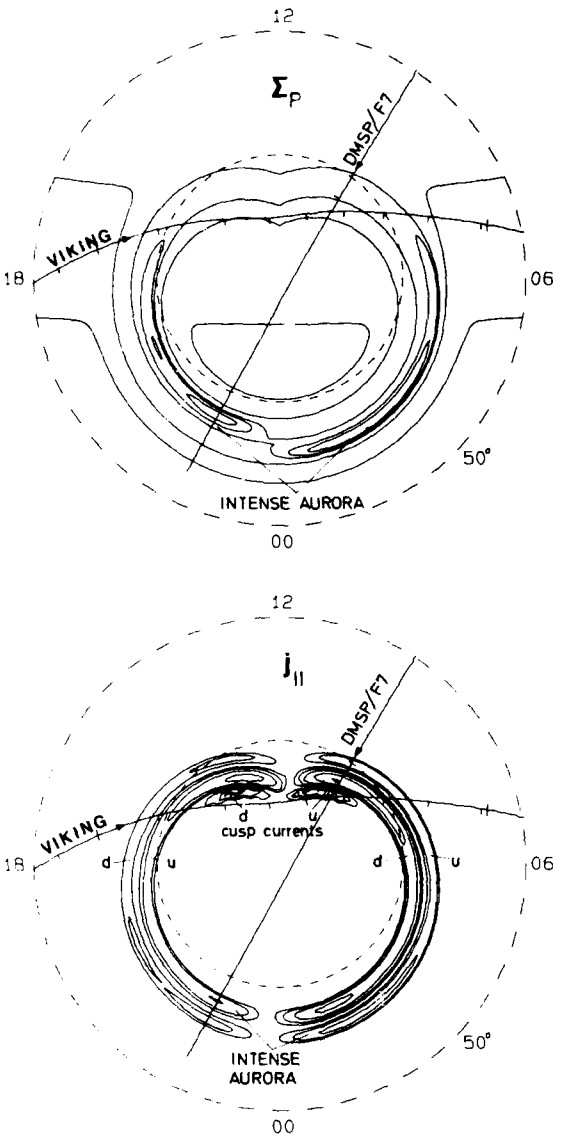

Fig. 2. Input Pedersen conductivity (Σ_P, top) and input field-aligned current ($j_\parallel$, bottom). Included are also the magnetic foot points of the Viking (dusk-dawn) and DMSP F7 (noon-midnight) satellites.

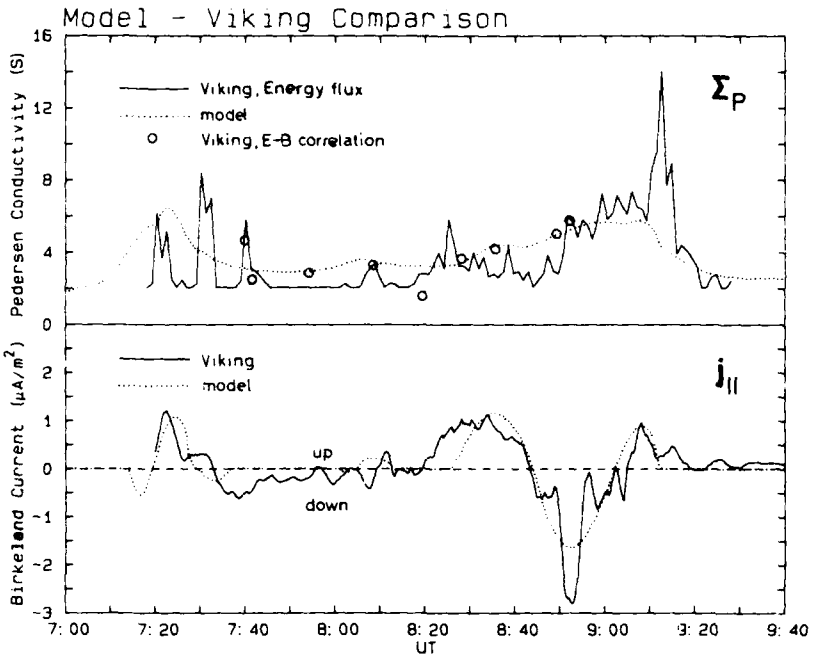

Fig. 3. Quantitative point-by-point comparison between model input data and Viking data along the ionospheric projection of the Viking orbit.

Figure 3 shows, at the top, the model and calculated height-integrated Pedersen conductivity profiles and, at the bottom, the model and calculated field-aligned current profiles along the ionospheric projection of the Viking orbit. The contribution to Σ_P from the measured particles has been estimated using the assumption that it is roughly proportional to the square root of the downward electron energy flux [*Harel et al.*, 1981] as described in section 2. The field-aligned current, $j_{||}$, has been estimated from the residual of the spin axis component of the magnetic field, b_3, shown in Figure 4 (bottom) and obtained by subtraction of the slow time variation of the background magnetic field.

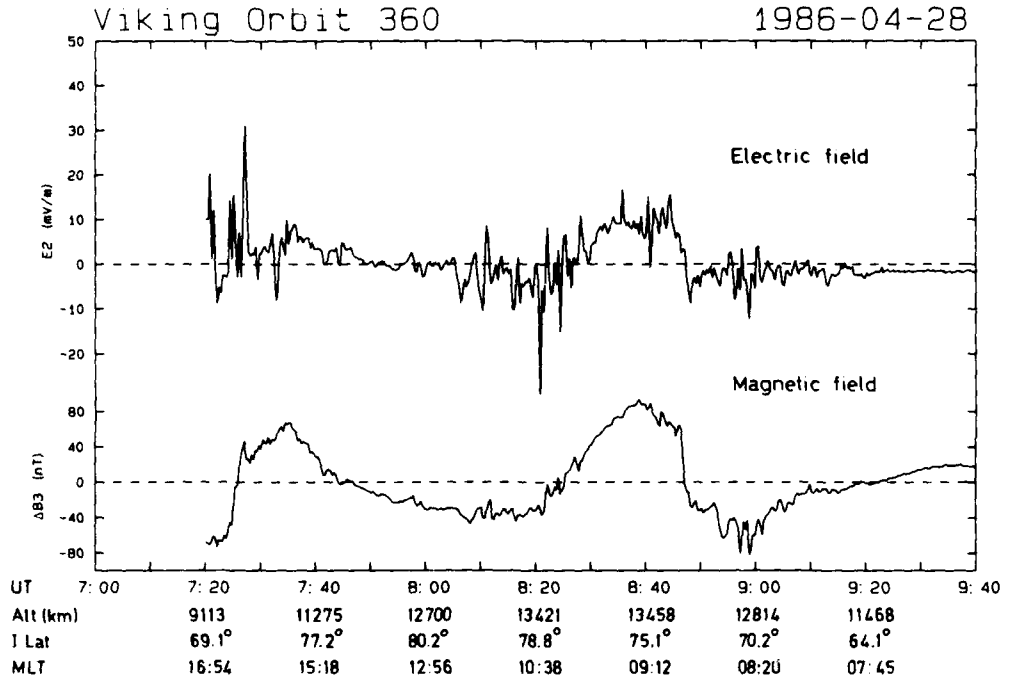

Fig. 4. Electric field (top) and magnetic field data (bottom) obtained for the dusk-dawn Viking orbit 360. For a definition of the coordinate system used, see *Block et al.* [1987]. E_2 corresponds roughly to the dawn-dusk electric field, and B_3 to the sunward magnetic field.

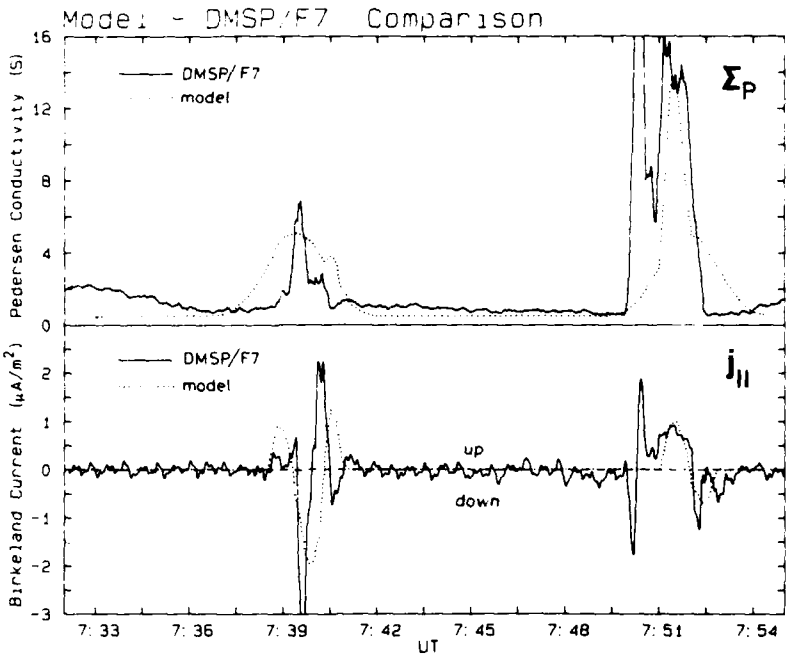

Fig. 5. Quantitative point-by-point comparison between model input data and DMSP F7 data along the ionospheric projection of the DMSP F7 orbit.

(This component contained the major part of the smaller-scale variations seen in the Viking magnetic field data.) For a definition of the coordinate system used, see *Block et al.* [1987]. The current values have been scaled using a dipole magnetic field approximation so that they refer to the ionospheric level. Note the clear large-scale correlation between the orthogonal electric field and magnetic field components in Figure 4 . This allows an independent estimate of the Σ_P variation (denoted by circles in Figure 3) as demonstrated by *Sugiura* [1984].

As can be seen, the Σ_P and $j_{||}$ profiles calculated from the Viking data are very well represented by the model data in terms of the relative magnitudes, widths, and locations of the major structures. Note that the calculated conductivity always has local maxima in the regions of upward field-aligned currents. This field-aligned current–conductivity coupling is a characteristic feature in auroral electrodynamics and has been taken into account here by using the linear relationship between $j_{||}$ and Σ, described by equation (10).

Figure 5 shows in a fashion similar to that in Figure 3 comparisons between the model field-aligned current and conductivity profiles and the corresponding estimates based on the DMSP F7 data. Here, too, the agreement is good concerning the large-scale variations. Consider for example the triple current sheet encountered around 0740 UT. The location and the integrated values of the upflowing and downflowing currents are very similar, although the width of the model current is slightly greater. As mentioned above, this triple current sheet was also traversed by the Viking satellite about 1 hour later. The magnitudes and signatures of the currents remain essentially the same during this 1-hour time period, with a value of 0.8 – 1 $\mu A/m^2$ for the region 2 upward current, 3 $\mu A/m^2$ for the region 1 downward current, and about 2 $\mu A/m^2$ for the upward cusp current. Thus, as far as one could judge from these observations, the dayside conditions seem to have been relatively stable even for the 1-hour time period preceding the DMSP F7 crossing.

For the nightside auroral crossing, the model conductivity and field-aligned current profiles, representing the intense auroral structure around 2130 MLT seen in the UV image, agree relatively well with the corresponding estimates based on the DMSP F7 data. The narrow structure at the poleward edge of the oval (0750 UT) is, however, not represented in the model. This may be just a local arc structure, or it may represent the poleward part of a multiple current sheet associated with the Harang discontinuity. Adopting the former interpretation, there is no reason to include small-scale structures in the model only along the satellite orbits where these can be detected and not elsewhere. The net current from these opposite currents is close to zero and will therefore not affect the results except very locally.

To summarise, the model input data are believed to rather accurately represent the real field-aligned current and conductivity distributions, as indicated by the good agreement with the measurements along the two different satellite orbits.

The equipotential distribution, calculated using the numerical model described in section 3 (equation (5)) and the input distributions presented above, is presented in Figure 6 in an inertial frame of reference. Superposed on this we have for comparison plotted the $\mathbf{E} \times \mathbf{B}$ drift vectors calculated from the Viking electric field (Figure 4) assuming that $\mathbf{E} \cdot \mathbf{B} = 0$. Note that the drift vectors are almost parallel to the convection streamlines everywhere except for two narrow regions, as will be discussed below.

The calculated convection pattern is of the normal two-cell type with a weak dusk cell displaced toward noon and a more intense, longitudinally extended and crescent-shaped dawn cell characteristic for the prevailing positive IMF B_y. The pattern is quite similar to the BC model of *Heppner*

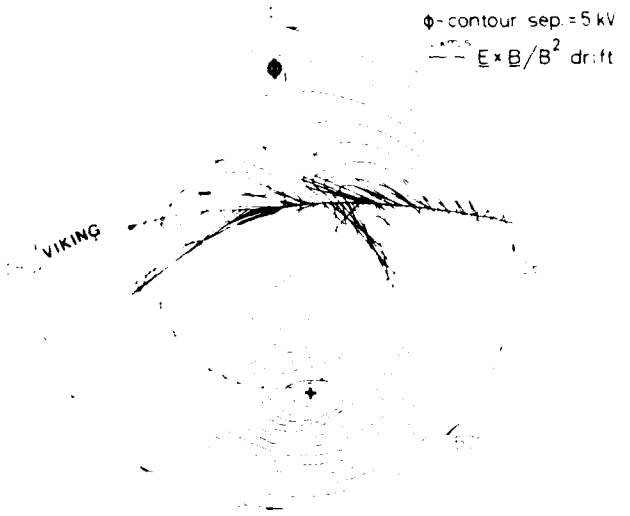

Fig. 6. Output potential distribution in the inertial frame. Contour separation is 5 kV. Along the Viking foot point (dusk–dawn) are shown the $\mathbf{E} \times \mathbf{B}$ drift vectors calculated from Viking electric field measurements.

and *Maynard* [1987], representing the most typical potential pattern encountered in the northern hemisphere for positive IMF B_y conditions and K_p in the range $3^+ \leq K_p \leq 4^-$ (same as in the present study). The main difference is that the equipotential contours of the statistical BC model are parallel to the 0900–2100 MLT meridian within almost the entire polar cap whereas the potential contours of the "instantaneous" pattern shown in Figure 6 change from being almost Sun-aligned on the dayside polar cap to aligned in the dawn–dusk direction on the nightside polar cap. Another difference is that the morning cell dominates more clearly over the evening cell for the "instantaneous" pattern.

Note the westward intrusion or clockwise rotation of the convection pattern close to midnight. Such a clockwise rotation is caused by the combined effect of intense field-aligned currents and polarization electric fields associated with the bright auroral intensifications there [*Marklund et al.*, 1985] as well as the day–night conductivity gradient [*Atkinson and Hutchison*, 1978]. The polar cap potential drop is about 60 kV, in good agreement with empirical values for the prevailing K_p-index [e.g., *Foster et al.*, 1986; *Heppner and Maynard*, 1987], and directed roughly between 0200–0300 MLT and 1500 MLT.

Figure 7 (bottom) shows the model and calculated potential profile along the ionospheric projection of the Viking orbit. This serves to demonstrate that the model results are not only qualitatively but also quantitatively in good agreement with the observations. Deviations occur, however, in two time intervals, most pronounced around 0830 UT and less clear around 0720 UT, where the high-altitude potential (Viking) has minima which are smaller or absent in the ionospheric (model) potential. It is evident from the measured field-aligned current profile (top) that intense upward currents are present in these regions. Furthermore, these regions show evidence of upward acceleration of ions as indicated by the inserted shaded areas. This is exemplified in Figure 8, which shows pronounced upward ion beams in the two highest-energy channels (0.52 keV and 1.25 keV) between 0720 and 0723 UT. In the downward current region between 0718 UT and 0720 UT, weak ion conics can be seen at the low-energy channel of 60 eV. The electron data (not shown here) show only weak acceleration signatures and are thus consistent with the upward ion beams observed essentially above the acceleration region. Another

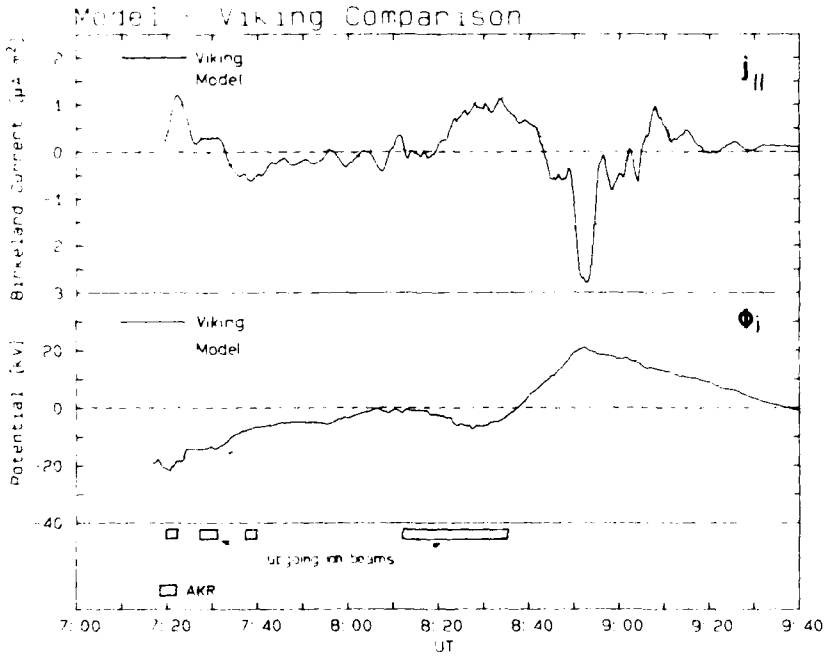

Fig. 7. Quantitative point-by-point comparison between model and observed potential profiles (middle) and between model and observed field-aligned currents (top) along the ionospheric projection of the Viking orbit. The shaded areas in the bottom indicate regions of upward accelerated ions and intense AKR.

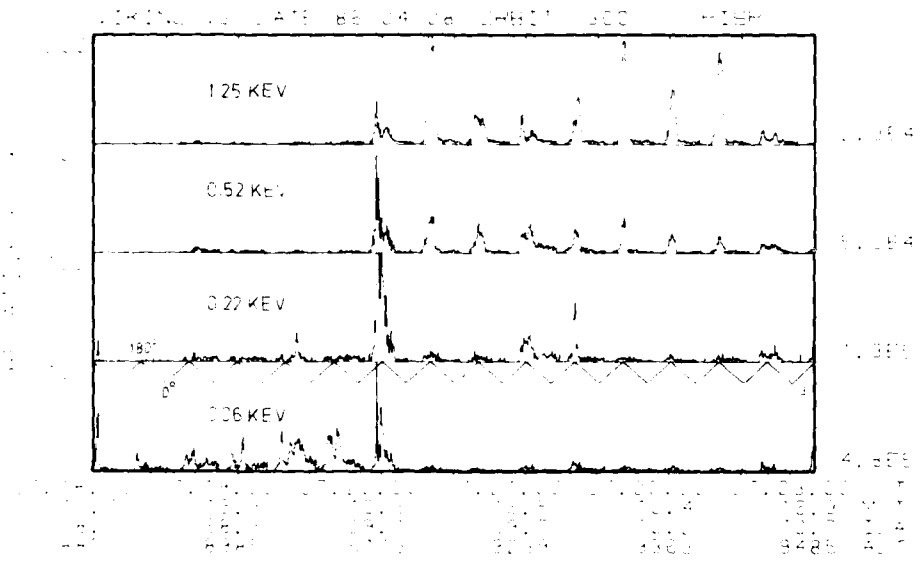

Fig. 8. Time series of ion fluxes at four selected energies (0.06, 0.22, 0.52, 1.25 k-V) obtained by the ion detectors (PISP1/2) on Viking. The ion fluxes are shown on a linear scale in relative units. The basic flux level in units of $(keV\ cm^2\ s\ sr)^{-1}$ is given at the right side of each panel. The pitch angle is indicated in the lowest panel. The ion fluxes are seen to be concentrated around 180° pitch angle (upward).

piece of evidence that Viking passed above an auroral acceleration region centered around 0720 UT is given by the high-frequency wave spectrogram in Figure 9. The electric component is shown here for the time interval between 0717:20 UT and 0722:10 UT. Intense auroral kilometric radiation (AKR) emissions centered around 0719:40 UT with low-frequency cutoffs between 350 and 400 kHz are seen at the top well above the electron gyrofrequency indicated

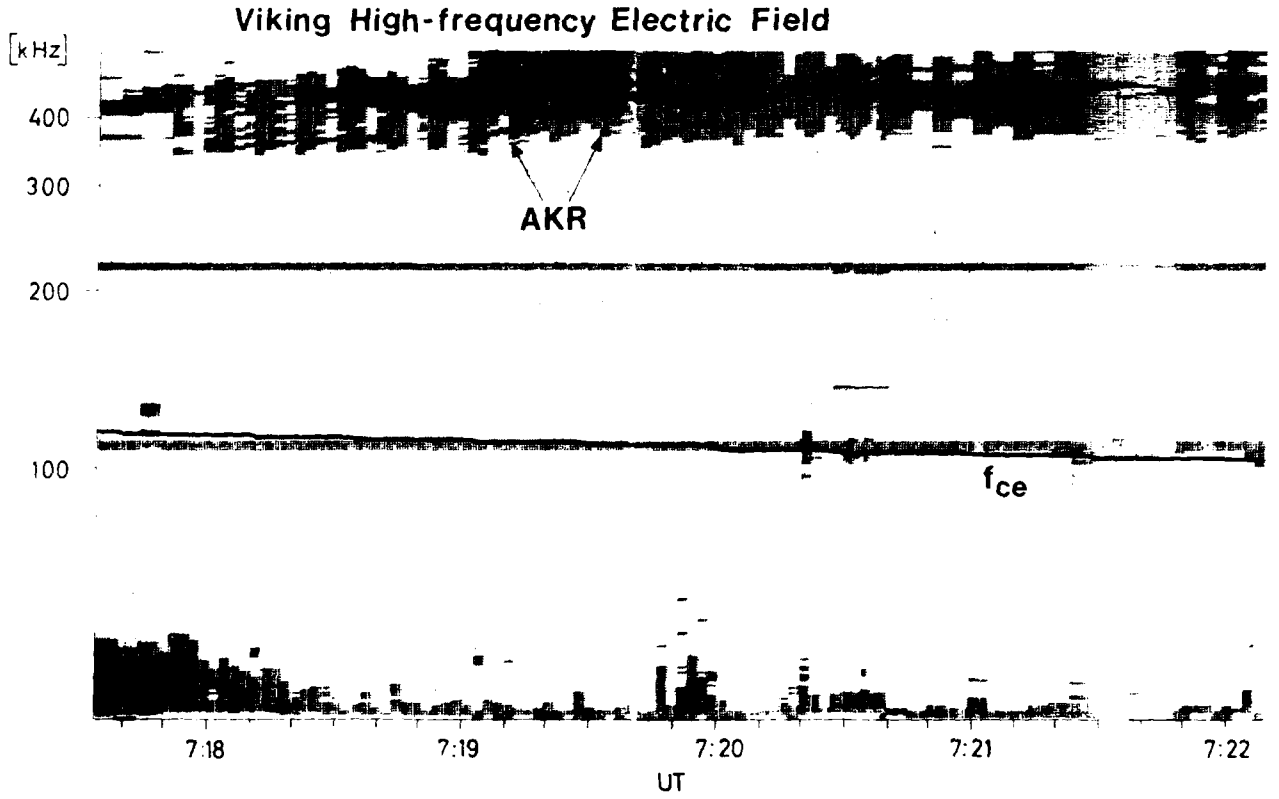

Fig. 9. Electric field observed by the high-frequency wave experiment on Viking during the afternoon auroral oval crossing around 0720 UT. Intense AKR emissions are seen at the top well above the electron gyrofrequency indicated by the solid line around 100 kHz. Impulsive hiss emissions are seen at the bottom, shortly before 0720 UT.

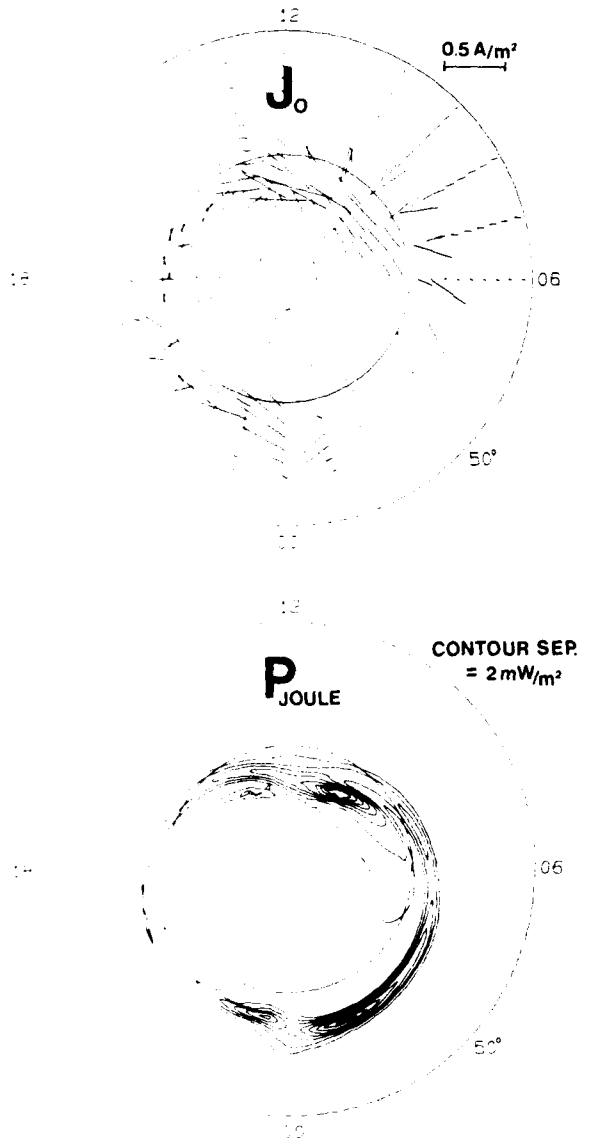

Fig. 10. The ionospheric current vectors, plotted every 2° of invariant latitude and every hour of magnetic local time (top), and Joule power dissipation (bottom) corresponding to the potential distribution shown in Figure 6 and conductivity distribution shown in Figure 2 (top).

by the solid line at around 100 kHz. Note also the impulsive character of the low-frequency hiss emissions around 0719:55 UT, which is characteristic for the crossing of an arc structure.

To summarize, the model output potential distribution agrees both qualitatively and quantitatively with the Viking observations, except in two regions where expected deviations occur, qualitatively consistent with upward parallel electric fields.

As a further illustration of the wide range of results that can be obtained with this model, Figure 10 shows the ionospheric current (top) and the Joule power dissipation (bottom) associated with this event and calculated from the model electric field and conductivity data using equations (1) and (11), respectively. Note the intense westward electrojet associated with the auroral activity close to magnetic midnight. These currents can be compared with currents that could be inferred from simultaneous ground-based magnetometer observations. The Joule power dissipation is seen to be concentrated into two regions: (1) the midnight sector and in particular the bright auroral structures there, and (2) the prenoon sector, characterized by relatively intense auroral structures seen by the UV imager and relatively intense field-aligned currents as measured by both the DMSP F7 and Viking.

A simplified picture of the magnetospheric convection is illustrated in Figure 11 (right), which is a projection of the deduced ionospheric two-cell convection pattern (left) to the equatorial plane using a dipole magnetic field. The location of the last closed equipotential contour (heavy line) is seen to correspond relatively well with that of the average plasmapause boundary (dotted line) as given by *Carpenter* [1966]. (Since the shape of the plasmapause varies, a detailed correspondence is not to be expected.)

6. Discussion

UV imaging of the aurora from polar-orbiting satellites such as Dynamics Explorer 1 and Viking represents an important new input to the study of auroral electrodynamics on a global scale. The images of the auroral oval provide not only a natural reference frame for the other observations but also valuable information on various electrodynamical parameters. It is, for example, evident that the observed variations in the UV emission intensities also reflect variations in the ionization and thus the ionospheric conductivity. This dependence has been used by, for example, *Craven et al.* [1983] and *Kamide et al.* [1986] to infer "instantaneous" conductivity distributions from DE 1 auroral images. A quantitative estimate involves, however, a number of uncertainties, as has been discussed in section 2.

It is also clear that active regions such as bright auroral structures are associated not only with enhanced conductivities but also with enhanced upward field-aligned currents. It is, however, very unclear how the information of the fine-scale structure seen in the weak and diffuse background oval could be used to better reconstruct the associated field-aligned current distribution. Therefore, it makes no sense to represent these fine-scale variations in the model input data unless it could be done not only for the conductivity but also for the field-aligned current.

For these reasons we have chosen an alternative and qualitative way of utilizing the UV image information, namely, to obtain a reference frame for the modeling and to identify the locations and extent of the major intense auroral structures, which are modeled by enhancements in the preexisting quiet time field-aligned current [*Iijima and Potemra*, 1976a, 1978] and conductivity distributions, here representative of the background auroral oval.

An important and new feature of the model presented here is that the field-aligned current and conductivity patterns are consistent with each other in the sense that the conductivity peaks in regions of upward field-aligned currents associated with the discrete aurora. To determine the exact form of such a correspondence is a very complicated problem since the precipitating particles creating enhanced ionisation are typically more energetic than those carrying the major part of the upward field-aligned currents. Qualitatively, such a correspondence is, however, well confirmed

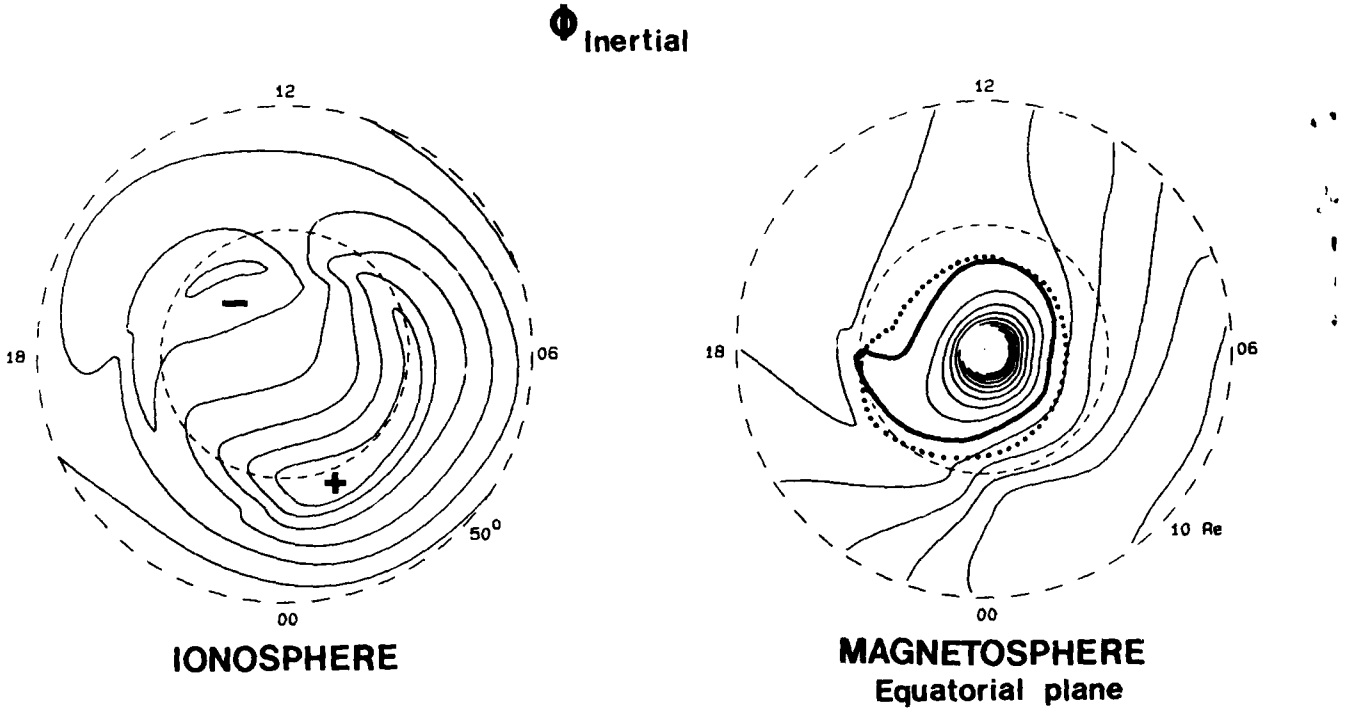

Fig. 11. The deduced two-cell convection pattern (left) and the corresponding magnetospheric convection (right) resulting from a simple projection to the equatorial plane using a dipole magnetic field. For comparison the average plasmapause from *Carpenter* [1966] has been inserted (dotted line).

from observations over auroral arcs. *Lyons et al.* [1979] found that when a field-aligned acceleration voltage (V) could be inferred from the electron spectra, the net downward electron energy flux generally varied as V^2 while the net upward field-aligned current was generally proportional to V. Since Σ_P is roughly proportional to the square root of the electron energy flux (see section 2 above), the relations above imply a direct proportionality between Σ_P and $j_\parallel$. A correspondence between these two parameters is also evident from Figures 3 and 5, which justifies our choice of the linear relationship described by equation (10).

The new method described in this paper is still under development, and refinements of some of the details in the model are to be expected as soon as we have gained more experience from several different events. The criteria used in the selection of a suitable event for a first study were that the entire auroral oval should be visible to the imager; that at least one large-scale auroral structure should exist in some local time sector of the oval; and that the substorm activity should be relatively stable during the time period for which the UV image is representative. The event chosen here from Viking orbit 360 was found to meet these various requirements reasonably well. The requirement of intense aurora implies, by definition, also substorm activity, which, as demonstrated by the *AE* index, was high but relatively stable (500 nT) during the time interval of 27 min for which the UV image is assumed to be representative.

For the dayside auroral region we do not see any problem with this assumption, since all information used to calibrate the model input data (from the Viking afternoon auroral oval crossing and the DMSP F7 prenoon auroral oval crossing) was obtained within 15 min. Since the triple field-aligned current sheets in the prenoon sector, as observed by DMSP F7 around 0739 UT and Viking about 1 hour later, had very similar characteristics (in terms of magnitudes, widths, etc.), the dayside activity might have been relatively stable even during the entire auroral oval transit time by Viking. This is also supported by the good agreement obtained between the model potential distribution and that inferred from the measurements (cf. Figures 6 and 7).

For the nightside auroral oval the requirement of roughly unchanged auroral conditions relative to those of the UV image during 27 min cannot be verified from the data set available here. We have assumed this to be the case, supported by the observations of intense particle fluxes and field-aligned currents in the region where the bright auroral intensification was observed by the UV imager half an hour earlier.

The global field-aligned current and conductivity distributions presented in Figure 2 and the corresponding equipotential pattern presented in Figure 6 are believed to represent the prevailing electrodynamical situation associated with the auroral situation illustrated by Figure 1 . The qualitative agreement between the model convection pattern and the $\mathbf{E} \times \mathbf{B}$ drift vectors and the good quantitative agreement between the model and calculated potential profile along the Viking orbit are a consequence of the careful selection of realistic global input data being calibrated to the Viking and DMSP F7 data. The asymmetry between the intense and crescent-shaped dawn convection cell (associated with the intense auroral activity and field-aligned currents) and the much weaker dusk convection cell shown in Figure 6 is consistent with earlier observations and theoretical predictions for positive IMF B_y conditions [*Heppner*, 1972; *Moser et al.*, 1974; *Crooker*, 1979].

It is interesting that the "instantaneous" potential pattern

calculated here from model input conductivity and field-aligned current distributions is quite similar to the average BC pattern of *Heppner and Maynard* [1987] based on a large statistical material of DE 2 electric field observations and representative for positive IMF B_y conditions and $3^+ \leq K_p \leq 4^-$ (representative also for Viking orbit 360). The average direction of the polar cap electric field between 0300–0400 MLT and 1500–1600 MLT, the polar cap potential drop of 60 kV, the dominant morning convection cell, and intrusion of the morning cell potential contours toward west in the nightside auroral oval and toward east in the dayside auroral oval are features which are characteristic for both the "instantaneous" and the statistical pattern.

In order to combine data from various satellites following the procedure outlined here a constructive assumption is that there is a perfect coupling between the electrodynamical parameters in the ionosphere and at satellite altitude. The good agreement between the measurements made at the two satellite altitudes, as well as between the measurements and the model input and output data, generally supports this assumption. As a result of using the assumption $\mathbf{E} \cdot \mathbf{B} = 0$ we found, however, in the regions of intense upward field-aligned currents, discrepancies between the model and calculated potentials (cf. Figures 6 and 7) indicative of upward parallel electric fields. *Weimer et al.* [1985] compared the electric field signatures at high and low altitudes as measured by the Dynamics Explorer 1 and 2 satellites. In agreement with the findings here they found that the large-scale characteristics of the electric fields at the two altitudes were very similar but that the small-scale electric field in the auroral zone had larger magnitudes at higher altitudes consistent with the existence of parallel electric fields.

The presence of upward accelerated ions and intense AKR emissions (0720 UT) well above the local electron gyrofrequency and absence of, or only weak, signatures of electron acceleration in these regions, all indicate that Viking passed above or crossed the upper part of the acceleration regions. For the two regions of upward field-aligned currents indicated in Figure 7 the potential drop amounts to about 5–10 kV, which is within the typical range of acceleration energies for the auroral particles.

The technique presented here is in principle applicable also to more disturbed and thus time-dependent events. Several UV images are then needed to follow the temporal evolution of the aurora as the satellite crosses over it. In this kind of time-dependent modeling, calibration to simultaneous measurements by several spacecraft is particularly useful.

7. SUMMARY

Simultaneous observations by the Viking and DMSP F7 satellites have been used in a new method to obtain snapshot pictures of the high-latitude electrodynamics associated with a specific auroral situation viewed by the UV imager experiment on Viking during orbit 360. The UV image was used to locate the regions of active intense auroras, which were represented by enhanced conductivities and upward field-aligned currents in the model input data. The global input distributions were calibrated so as to be quantitatively consistent with the conductivity and field-aligned current profiles calculated from the particle and magnetic field data along the two satellite orbits. These distributions were used together with Ohm's law to solve for the ionospheric potential distribution, which was finally tested against the electric field observed by Viking. The results can be summarized as follows:

1. The model input data (Σ and $j_\parallel$) are qualitatively consistent with the auroral imager data and quantitatively consistent with the Viking and DMSP F7 observations. An important feature in the model is a current ($j_\parallel$)-conductivity coupling term.

2. There is a good agreement both qualitatively between the output potential distribution and the observed $\mathbf{E} \times \mathbf{B}$ drift and between the two corresponding potential profiles along the Viking orbit. The "instantaneous" potential distribution is, further, quite similar to the empirical BC model of *Heppner and Maynard* [1987] based on DE 2 electric field data from periods of positive IMF B_y and $3^+ \leq K_p \leq 4^-$, which is the same conditions as for the event studied here.

3. Potential differences between the Viking altitude and the ionosphere indicative of upward parallel electric fields are found for two time periods corresponding to Viking crossings above acceleration regions further characterized by upgoing ions, intense upward field-aligned currents, and intense AKR emissions.

4. To illustrate the variety of model results that can be obtained, the ionospheric currents, Joule power dissipation, and magnetospheric convection representative for this event have been estimated using the model conductivity and potential distributions. An equatorial plane projection of the potential pattern shows for the last closed equipotential contour a good agreement with the average location of the plasmapause.

Acknowledgments. The authors are grateful to C.-G. Fälthammar, L. Block, and P.-A. Lindqvist, The Royal Institute of Technology; R. Erlandson, The Johns Hopkins University; R. Elphinstone, University of Calgary; E. Friis-Christensen, Danish Meteorological Institute; R. Heelis, The University of Texas at Dallas; and P. Rothwell, Air Force Geophysics Laboratory, for valuable comments and helpful discussions. This research was supported by the Swedish Board for Space Activities. The Viking Project is managed and operated by the Swedish Space Corporation under contract from the Swedish Board for Space Activities. The Viking magnetic field experiment was supported by the Office of Naval Research. We wish to thank in particular the engineering team of the Space Group of the Department of Plasma Physics, The Royal Institute of Technology, for their competent work in constructing and testing the Viking electric field experiment. The assistance of NASA in providing the flux gate magnetometer sensor for the DMSP F7 magnetic field experiment is gratefully acknowledged. We are grateful to the JHU/APL Space Department for constructing and testing the DMSP F7 and Viking magnetic field experiments.

The Editor thanks two referees for their assistance in evaluating this paper.

REFERENCES

Atkinson, G., and D. Hutchison, Effect of the day night ionospheric conductivity gradient on polar cap convective flow, *J. Geophys. Res.*, *83*, 725–729, 1978.

Bleuler, E., C. H. Li, and J. S. Nisbet, Relationships between the Birkeland currents, ionospheric currents, and electric fields, *J. Geophys. Res.*, *87*, 757–776, 1982.

Block, L. P., C.-G. Fälthammar, P.-A. Lindqvist, G. Marklund, F. S. Mozer, A. Pedersen, T. A. Potemra, and L. J. Zanetti, Electric field measurements on Viking: First results, *Geophys. Res. Lett.*, *14*, 435–438, 1987.

Blomberg, L. G., and G. T. Marklund, The influence of conductivities consistent with field-aligned currents on high-latitude convection patterns, *J. Geophys. Res.*, in press, 1988a.

Blomberg, L. G., and G. T. Marklund, A numerical model of ionospheric convection derived from field-aligned currents and the corresponding conductivity, *Rep. TRITA-EPP-88-03*, Royal Inst. of Technol., Stockholm, 1988b.

Carpenter, D. L., Whistler studies of the plasmapause in the magnetosphere, 1, Temporal variations in the position of the knee and some evidence on plasma motions near the knee, *J. Geophys. Res.*, *71*, 693–710, 1966.

Craven, J. D., Y. Kamide, L. A. Frank, S.-I. Akasofu, and M. Sugiura, Distribution of aurora and ionospheric currents observed simultaneously on a global scale, in *Magnetospheric Currents*, *Geophys. Monogr. Ser.*, vol. 28, edited by T. A. Potemra, pp. 137–146, AGU, Washington, D. C., 1983.

Crooker, N. U., Dayside merging and cusp geometry, *J. Geophys. Res.*, *84*, 951–959, 1979.

Foster, J. C., J. M. Holt, R. G. Musgrove, and D. S. Evans, Ionospheric convection associated with discrete levels of particle precipitation, *Geophys. Res. Lett.*, *13*, 656–659, 1986.

Harel, M., R. A. Wolf, P. H. Reiff, R. W. Spiro, W. J. Burke, F. J. Rich, and M. Smiddy, Quantitative simulation of a magnetospheric substorm, 1, Model logic and overview, *J. Geophys. Res.*, *86*, 2217–2241, 1981.

Heelis, R. A., J. C. Foster, O. de la Beaujardière, and J. Holt, Multistation measurements of high-latitude ionospheric convection, *J. Geophys. Res.*, *88*, 10111–10121, 1983.

Heppner, J. P., Polar cap electric field distributions related to the interplanetary magnetic field direction, *J. Geophys. Res.*, *77*, 4877–4887, 1972.

Heppner, J. P., and N. C. Maynard, Empirical high-latitude electric field models, *J. Geophys. Res.*, *92*, 4467–4489, 1987.

Hultqvist, B., Auroral particles, in *Cosmical Geophysics*, edited by A. Egeland, Ø. Holter, and A. Omholt, pp. 161–179, Scandinavian University Books, Oslo, 1973.

Iijima, T., and T. A. Potemra, The amplitude distribution of field-aligned currents at northern high latitudes observed by Triad, *J. Geophys. Res.*, *81*, 2165–2174, 1976a.

Iijima, T., and T. A. Potemra, Field-aligned currents in the dayside cusp observed by Triad, *J. Geophys. Res.*, *81*, 5971–5979, 1976b.

Iijima, T., and T. A. Potemra, Large-scale characteristics of field-aligned currents associated with substorms, *J. Geophys. Res.*, *83*, 599–615, 1978.

Kamide, Y., and S. Matsushita, Simulation studies of ionospheric electric fields and currents in relation to field-aligned currents, 1, Quiet periods, *J. Geophys. Res.*, *84*, 4083–4098, 1979a.

Kamide, Y., and S. Matsushita, Simulation studies of ionospheric electric fields and currents in relation to field-aligned currents, 2, Substorms, *J. Geophys. Res.*, *84*, 4099–4115, 1979b.

Kamide, Y., J. D. Craven, L. A. Frank, B.-H. Ahn, and S.-I. Akasofu, Modeling substorm current systems using conductivity distributions inferred from DE auroral images, *J. Geophys. Res.*, *91*, 11235–11256, 1986.

Lyons, L. R., and R. L. Walterscheid, Feedback between neutral winds and auroral arc electrodynamics, *J. Geophys. Res.*, *91*, 13506–13512, 1986.

Lyons, L. R., D. S. Evans, and R. Lundin, An observed relation between magnetic field aligned electric fields and downward electron energy fluxes in the vicinity of auroral forms, *J. Geophys. Res.*, *84*, 457–461, 1979.

Marklund, G. T., M. A. Raadu, and P.-A. Lindqvist, Effects of Birkeland current limitation on high-latitude convection patterns, *J. Geophys. Res.*, *90*, 10864–10874, 1985.

Marklund, G. T., R. A. Heelis, and J. D. Winningham, Rocket and satellite observations of electric fields and ion convection in the dayside auroral ionosphere, *Can. J. Phys.*, *64*, 1417–1425, 1986.

Marklund, G. T., L. G. Blomberg, T. A. Potemra, J. S. Murphree, F. J. Rich, and K. Stasiewicz, A new method to derive "instantaneous" high-latitude potential distributions from satellite measurements including auroral imager data, *Geophys. Res. Lett.*, *14*, 439–442, 1987.

Mishin, V. M., S. B. Lunyushkin, D. Sh. Shirapov, and W. Baumjohann, A new method for generating instantaneous ionospheric conductivity models using ground-based magnetic data, *Planet. Space Sci.*, *34*, 713–722, 1986.

Mozer, F. S., W. D. Gonzalez, F. Bogatt, M. C. Kelley, and S. J. Schutz, High-latitude electric fields and the three-dimensional interaction between the interplanetary and terrestrial magnetic fields, *J. Geophys. Res.*, *79*, 56–63, 1974.

National Space Science Data Center, Provisional auroral electrojet indices for March–June 1986, *PROMIS Ser.*, vol. 2, *Publ. 86-16*, World Data Center C2, Greenbelt, Md., 1986.

Nisbet, J. S., M. J. Miller, and L. A. Carpenter, Currents and electric fields in the ionosphere due to field-aligned auroral currents, *J. Geophys. Res. 83*, 2647–2657, 1978.

Rees, M. H., Auroral ionozation and excitation by incident energetic electrons, *Planet. Space Sci.*, *11*, 1209–1217, 1963.

Reiff, P. H., Models of auroral-zone conductances, in *Magnetospheric Currents*, *Geophys. Monogr. Ser.*, vol. 28, edited by T. A. Potemra, pp. 180–191, AGU, Washington, D. C., 1984.

Sugiura, M., A fundamental magnetosphere–ionosphere coupling mode involving field-aligned currents as deduced from DE-2 observations, *Geophys. Res. Lett.*, *11*, 877–880, 1984.

Vickrey, J. F., R. R. Vondrak, and S. J. Matthews, The diurnal and latitudinal variation of auroral zone ionospheric conductivity, *J. Geophys. Res.*, *86*, 65–75, 1981.

Wallis, D. D., and E. E. Budzinski, Empirical models of height-integrated conductivities, *J. Geophys. Res.*, *86*, 125–137, 1981.

Weimer, D. R., C. K. Goertz, D. A. Gurnett, N. C. Maynard, and J. L. Burch, Auroral zone electric fields from DE 1 and 2 at magnetic conjunctions, *J. Geophys. Res.*, *90*, 7479–7494, 1985.

L. G. Blomberg and G. T. Marklund, Department of Plasma Physics, Royal Institue of Technology, S-100 44 Stockholm, Sweden.

D. A. Hardy and F. J. Rich, Space Physics Division, Air Force Geophysics Laboratory, Bedford, MA 01731.

J. S. Murphree, Department of Physics, University of Calgary, Calgary, Alberta, Canada T2N 1N4.

T. A. Potemra and L. J. Zanetti, Applied Physics Laboratory, Johns Hopkins University, Laurel, MD 20707.

R. Pottelette, Centre de Recherches en Physique de l'Environnement Terrestre et Planétaire, 4 Avenue de Neptune, F-94107 Saint-Maur-des-Fossés Cedex, France.

K. Stasiewicz, Swedish Institute of Space Physics, Uppsala Division, S-755 90 Uppsala, Sweden.

(Received December 1, 1987;
revised May 23, 1988;
accepted June 21, 1988.)